AGU PUBLICATIONS

JGR

Journal of Geophysical Research: Space Physics

RESEARCH ARTICLE
10.1002/2017JA024499

Key Points:
- Developed criteria for selection of SKR low-frequency extensions based on analysis of 2006 RPWS data
- Categorized into short LFEs (<20 h) associated with tail reconnection and long events (>20 h) associated with solar wind dynamics
- We conclude that short LFEs are a good proxy for reconnection in the tail

Supporting Information:
- Supporting Information S1
- Figure S1
- Figure S2

Correspondence to:
J. J. Reed,
jr1e13@soton.ac.uk

Citation:
Reed, J. J., Jackman, C. M., Lamy, L., Kurth, W. S., & Whiter, D. K. (2018). Low-frequency extensions of the Saturn Kilometric Radiation as a proxy for magnetospheric dynamics. *Journal of Geophysical Research: Space Physics*, *123*. https://doi.org/10.1002/2017JA024499

Received 21 JUN 2017
Accepted 20 DEC 2017
Accepted article online 4 JAN 2018

Low-Frequency Extensions of the Saturn Kilometric Radiation as a Proxy for Magnetospheric Dynamics

J. J. Reed[1], C. M. Jackman[1], L. Lamy[2], W. S. Kurth[3], and D. K. Whiter[1]

[1]Department of Physics and Astronomy, University of Southampton, Southampton, UK, [2]Observatoire de Paris, Meudon, France, [3]Department of Physics and Astronomy, University of Iowa, Iowa City, IA, USA

Abstract Saturn Kilometric Radiation (SKR) is an auroral radio emission which can be detected quasi-continuously by the Cassini spacecraft. It has been shown to respond to magnetotail reconnection and to changes in solar wind conditions and thus offers the potential to be used as a remote proxy for magnetospheric dynamics. This work has developed criteria for the selection of low-frequency extensions (LFEs), powerful intensifications of the main SKR emission, accompanied by an expansion of the SKR to lower frequencies. Upon examination of data from the Cassini Radio and Plasma Wave Science instrument, we detect 282 LFE events which are further grouped into two categories. Shorter events (<20 h) associated with tail reconnection have a median waiting time of ~10 h, a median duration of 3.1 h and a strong correlation with the northern and southern SKR phase systems. The 60% of the short LFEs have a reconnection event within the preceding 6 h. Longer events (>20 h), associated with increases in solar wind dynamic pressure, can last multiple planetary rotations, have a median waiting time of ~20 days, and show no relationship with SKR phase. An analysis of the power emitted during LFEs suggests that tail reconnection is not always observed or detected in situ which may partially explain the low correlation between LFEs and tail reconnection. We conclude that short LFEs are a good proxy for reconnection in the tail.

1. Introduction

The Saturn Kilometric Radiation (SKR) was originally detected by Voyager 1 (Kaiser et al., 1980). The typical frequency range is from 3 kHz to 1.2 MHz, peaking between 100 and 400 kHz (Kaiser & Desch, 1984; Lamy et al., 2008). The SKR is quasi-continuous and is generated via the cyclotron maser instability (CMI) (Lamy, Schippers, et al., 2010; Lamy et al., 2011; Mutel et al., 2010; Menietti et al., 2011; Wu & Lee, 1979) on field lines near the auroral regions. The CMI process involves the beaming of a radio emission excited by energetic (1–20 keV Cowley et al., 2004) auroral electrons via cyclotron resonance at frequencies close to the local electron cyclotron frequency, $f_c = qB/(2\pi m)$, where q is the electron charge, B is the local magnetic field strength, and m is the electron mass. The frequency of the emission is proportional to the strength of the local magnetic field of the source and is therefore inversely proportional to the height of the source cubed ($1/R^3$). Lamy, Schippers, et al. (2010) showed the difference between the SKR emission frequency and the local electron cyclotron frequency to be less than 2% and so, using an internal magnetic field model by Dougherty (2005); Kimura et al. (2013) showed that the peak emission of the SKR (between 100 and 400 kHz) originates from sources between 0.5 and 1.5 R_S from the planet (1 R_S = 60, 268 km). The SKR can extend down to 10 kHz or below, which equates to a source region at 5 R_S or further.

The SKR intensifies periodically with the rotation of Saturn as a source region passes through the morning local time (LT) sector (Gurnett, 2005; Mitchell et al., 2009). Lamy et al. (2013) showed that this behavior is common between multiple wavelength emissions and is found in the radio, UV, and IR aurorae. At Earth (Lamy, Zarka, et al., 2010) and Jupiter (Zarka & Genova, 1983) the peaks in the auroral radio emissions are fixed in period and related to the rotation of the planet. At Saturn this is not the case, where the periodicity of regularly pulsed SKR was found to have changed significantly between the measurements by Voyager and those of Ulysses and Cassini 20 years later (Galopeau & Lecacheux, 2000; Gurnett, 2005). This change was too large to be due to a change in the rotation of the deep interior (Gurnett et al., 2007), and thus, the link between the SKR and the true rotation rate of Saturn remains a topic of much debate. We now know that not only does the period between the SKR peaks change over time, there are also distinct separate periods associated with the northern

and southern hemispheres (Gurnett et al., 2009). From Cassini Radio and Plasma Wave Science (RPWS) data Lamy (2011) derived the time-dependent northern and southern SKR phase systems. In these systems, a phase of 0° indicates the timing of the SKR maxima and the passing of an active source region through 8 h LT.

Since Voyager, the SKR period has been found to vary over a range of time scales. Zarka et al. (2007) noted a correlation between the solar wind dynamic pressure and short-term variation of the SKR periodicity. The season of the planet also has a long-term effect on the period of the SKR (Cowley & Provan, 2016; Galopeau & Lecacheux, 2000; Gurnett et al., 2009, 2010; Gurnett, 2011; Kurth et al., 2008). For example, prior to Saturn equinox (August 2009), there were two clear periods for the longer southern SKR system and the shorter northern SKR system (Gurnett et al., 2010; Lamy, 2011). As equinox approached the two periods converged and remained close to each other until 2012 (Fischer et al., 2015; Provan et al., 2014) before they finally crossed in mid-2013 and diverged after until late 2015 (Provan et al., 2016; Ye et al., 2016).

In addition to the variations in period, the SKR intensity varies over a wide range of time scales. The solar wind dynamic pressure has been shown to affect not only the intensity of the SKR (Badman et al., 2008; Desch & Kaiser, 1981; Desch, 1982; Desch & Rucker, 1983; Taubenschuss et al., 2006) but also the beaming of the SKR by extending the spatial size of the source region in longitude/latitude. In Clarke et al. (2005) it was noted that following a solar wind compression the SKR intensified and the usual rotational modulation was disrupted; however, Kurth et al. (2005) found that Ulysses saw SKR during this same interval suggesting that the compression had indeed changed the beaming of the SKR causing Cassini to miss it. Kimura et al. (2013) showed that SKR intensity is correlated with both solar EUV flux and solar wind dynamic pressure which vary within a solar cycle.

The RPWS spectrum contains several features. The main band is the region between 100 and 400 kHz of the SKR spectrum. This region is quasi-continuous and is formed via the CMI. In addition, there are two lower frequency narrowband components separate to the main band and not linked and with the SKR, the narrowband-Saturnian Myriametric Radiation (n-SMR) and the narrowband-SKR (n-SKR). They are believed to be formed by wave mode conversions at density changes in the inner or outer region of the plasma disk near the equatorial plane (Louarn et al., 2007; Wang et al., 2010; Ye et al., 2009, 2010). The n-SMR exists below 10 kHz and appears to slightly supercorotate relative to the rotation of Saturn (in comparison to the Saturn Longitude System derived by Kaiser et al., 1980, based on Voyager 1 radio measurements, Louarn et al., 2007). It was also associated with "energetic events" in the magnetosphere. The n-SKR is less intense than the SKR and n-SMR and lies between 10 and 40 kHz (although it can go down to 3 kHz) (Lamy et al., 2008) peaking around 20 kHz. Wang et al. (2010) found that both emissions occur 1 to 2 days after an intensification of the SKR as had previously been observed for the 5 kHz emission by Louarn et al. (2007).

The features that we will be focusing on in this study are SKR low-frequency extensions (LFEs), an expansion of the entire kilometric spectrum and in particular of the main band from high to low frequencies. An LFE is a signature of a global intensification of the SKR spectrum and, like the quasi-continuous higher-frequency SKR, is produced via the CMI mechanism. LFEs were studied in particular detail by Jackman, Lamy, et al. (2009) who correlated them with episodes of magnetotail reconnection at Saturn and associated them with an extension of the radio source to higher altitudes along the field lines. They suggested that following reconnection, field-aligned currents are set up whose electron density exceeds that which can be carried by the plasma without greater acceleration. This leads to a taller acceleration region, where the "top" is farther up the field line and may coincide with a SKR source region at correspondingly large distances. Here the magnetic field strength will be lower; hence, the cyclotron maser will produce radio emissions at lower frequencies. At Earth the acceleration region and the CMI source region coincide as the former is required to produce a plasma cavity devoid of cold plasma and thus the conditions for CMI to operate. At Saturn the plasma may already be low enough density to allow the CMI to operate without the acceleration region, but the exact link between the acceleration region and the source region is not well understood.

Several authors have sought to examine the link between Saturn's rotation and magnetospheric dynamics. It had previously been suggested that plasmoid release occurs once every planetary rotation (Burch et al., 2008), but Jackman, Arridge, et al. (2009) used a more appropriate coordinate system for examining reconnection and found this not to be the case. More recently, Jackman et al. (2016) looked at the dependence of plasmoid occurrence on the rotation of the planet by comparing a catalogue of 65 plasmoid events detected in 2006 to the northern and southern magnetic phase systems (Andrews et al., 2010; Provan et al., 2009) (a similar concept to the SKR phase systems but which instead tracks the rotations of the northern

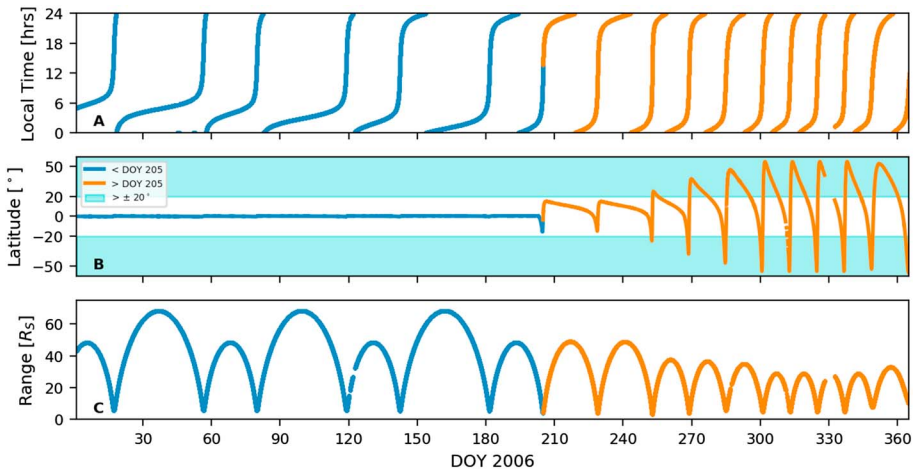

Figure 1. (a) Local time, (b) latitude, and (c) radial distance of Cassini from Saturn in R_S. The location traces are split between pre (blue) and post (orange) DOY 205 when Cassini changed to a higher-latitude trajectory. We separated our data into regions where the spacecraft latitude was less than | 20° | and where the latitude is greater than |20° |. The latter region is marked by the cyan shaded regions in Figure 1b.

and southern hemispheric current systems on top of a corotational current system that cause radially propagating perturbations in the magnetic field of Saturn). They found that the events preferentially occur when the northern and southern magnetic systems are in antiphase a condition which had been previously associated with the outward displacement of plasma (Burch et al., 2009; Clarke, Andrews, Arridge, et al., 2010; Clarke, Andrews, Coates, et al., 2010; Hunt et al., 2014, 2015) and a thin current sheet (Provan et al., 2012). Kennelly et al. (2013) analyzed injection events (where hotter, less dense plasma moves toward the inner magnetosphere) from July 2004 to December 2011. While there was no correlation found for the set of all events, they found that events observed near midnight local time are strongly ordered by the SKR-derived Saturnian Longitude System 4 (SLS4) (Gurnett, 2011). This ordering varied with the Saturnian season, being stronger with the northern SKR system preequinox and stronger with the southern SKR system in the postequinox era.

Through examining long intervals of SKR data the aims of this study are to automate the search for LFEs so that a large statistical base can be built up and to examine their properties and their use as a proxy for magnetospheric dynamics. We focus our statistical search on Cassini data from 2006 due to the deep tail orbits and good spacecraft local time and latitude coverage. These factors have also made 2006 of interest to those looking at magnetotail dynamics and as such there is a large catalogue of tail reconnection events that we can compare to. Jackman, Lamy, et al. (2009) defined LFEs based on intensification and the change in frequency of the emission somewhat arbitrarily. For this work we make this identification process more robust, by statistically examining the SKR spectrum for significant departures from "average" behavior. In section 2 we discuss the data set used, while section 3 outlines the criteria for detecting LFEs. Sections 4–6 discuss the properties of LFEs such as their latitudinal and local time visibility (section 4), the properties of a subset of the LFEs associated with solar wind dynamics (section 5), and the non–solar wind-associated LFEs (section 6). Section 7 examines the relationship of the LFEs with known reconnection events.

2. Data

For this paper we combine various data sets from the Cassini spacecraft at Saturn in 2006. Cassini's orbit in 2006 gave good tail coverage in terms of local time and latitude (see Figure 1) as well as containing the deepest tail orbits of the Cassini mission (out to 68 R_S). Processed RPWS data (Gurnett et al., 2004) are used to develop a criterion for selecting LFEs. We then use Cassini Magnetometer (Dougherty et al., 2004) data, a catalogue of reconnection events (Smith et al., 2016) (hereafter S16), the northern and southern SKR phase systems (Lamy, 2011) and modeled solar wind data from Michigan Solar Wind Model (mSWiM) (Zieger & Hansen, 2008), to examine multiple aspects of magnetospheric dynamics.

We use a high-resolution (90 s) power time series integrated over the 40–100 kHz and 100–600 kHz spectral bands for 2006 in order to develop our criteria for selecting LFEs. The power is given in W sr^{-1}. We also

use a high-resolution (90 s) data set consisting of the intensity of the observed radio waves as a function of time and frequency for comparison with our power data set to ensure we are selecting events that represent low-frequency extensions. This flux intensity is given in units of W m^{-2} Hz^{-1} and normalized to 1 astronomical unit (AU). These data sets are similar to those derived by Lamy et al. (2008) using RPWS data, which is based on previous work by Zarka et al. (2004) and Cecconi and Zarka (2005). Our data set differs slightly from the data set used by Lamy et al. (2008) in that whereas they placed a circular polarization ($|V| > 0.8$) and a signal-to-noise ratio (>10 dB) criteria, we have no criterion placed on the circular polarization. The 100–600 kHz range is selected to include the main band region of the SKR (100–400 kHz). The 40–100 kHz range is selected to include the region below the main band where a low-frequency extension would extend in to, the lower limit of 40 kHz being selected to limit the pollution from narrowband emissions.

In order to assess the use of LFEs as a proxy for magnetospheric dynamics, we use the S16 catalogue of 2,094 dipolarization, plasmoids, and traveling compression regions (TCRs) detected during 2006. Many of these events occur in chains, with multiple reconnection signatures observed within 3 h of each other. These chain events were deemed in S16 to represent multiple signatures of magnetic field reconfiguration likely linked to the same episode of reconnection. We thus suggest that chain events may be linked to a single response of the SKR and hence we only consider the first event out of each chain. This left a total of 234 plasmoids, TCRs, and dipolarization detected between day of year (DOY) 1 and 282 of 2006 as the in situ viewing conditions for reconnection events changed significantly toward the end of the year. Using the mSWiM model, which propagates measurements of various solar wind parameters taken near Earth to the orbit of Saturn, we are also able to compare our LFE catalogue with simultaneous solar wind behavior.

To investigate the relationship between the occurrence of LFEs and the SKR phase, we use the phase data set developed by Lamy (2011) that organizes SKR maxima. They used Lomb-Scargle analysis, a technique employed to perform spectral analysis of noncontinuous data, over a 6 year period from 2004 to 2010 to find the SKR period and related phase systems for each hemisphere. The northern and southern emissions were separated by their circular polarizations (left handed for southern and right handed for northern) allowing individual periods to be found and phase systems defined. Each hemispheric phase system has a phase of 0/360° when the respective SKR emission reaches its peak.

2.1. Visibility of SKR

The visibility of the SKR varies with spacecraft local time, latitude, and radial distance. Due to the coned beaming of the emission from the high-latitude northern and southern source regions, there exists an equatorial radio shadow zone with the furthest extent at 6–7 R_S for frequency range 80–900 kHz (Lamy et al., 2008). Figure 7 of Lamy et al. (2008) is a 2-D schematic of the equatorial shadow zone. For given sources in the northern and southern hemisphere at height, h, the emissions are beamed in two cones centered on their respective field lines. This leads to the equatorial shadow zone (additionally, Figure 11 from Lamy et al. (2008) shows SKR spectra as a function of spacecraft local time and latitude based on 2.75 years of RPWS observations). While the SKR is observed from all local times, the maximum intensity and bandwidth are recorded on the morning side between 02 h and 08 h with weakest emissions between 16 h and 20 h. Most of the SKR is observed between latitudes of −20° and +60° (Lamy et al., 2008; Kimura et al., 2013), while at latitudes greater than ±20° the visibility of the lower frequencies increases. Due to this variability with the location of the observer, our criteria for selecting LFEs are dependent on spacecraft location.

3. Automated Detection of Low-Frequency Extensions

3.1. Criteria

We now discuss our criteria for automatically selecting low-frequency extension features from the SKR. We examined the behavior of the SKR throughout 2006, including the statistical variations in power and emission frequency and used this to identify a training set of LFEs by visual inspection. We then developed criteria that best picked out these types of events. When trying to identify a LFE we were looking for three features that needed to be quantified: (1) An intensification in the higher-frequency region, (2) a significant extension of the emission down to lower frequencies, and (3) an intensification at these lower frequencies (the second and third features being closely linked). In developing these criteria we account for the significant variation of SKR visibility with both spacecraft local time and latitude as has been shown by several previous studies including Lamy et al. (2008), Kimura et al. (2013), and discussed above.

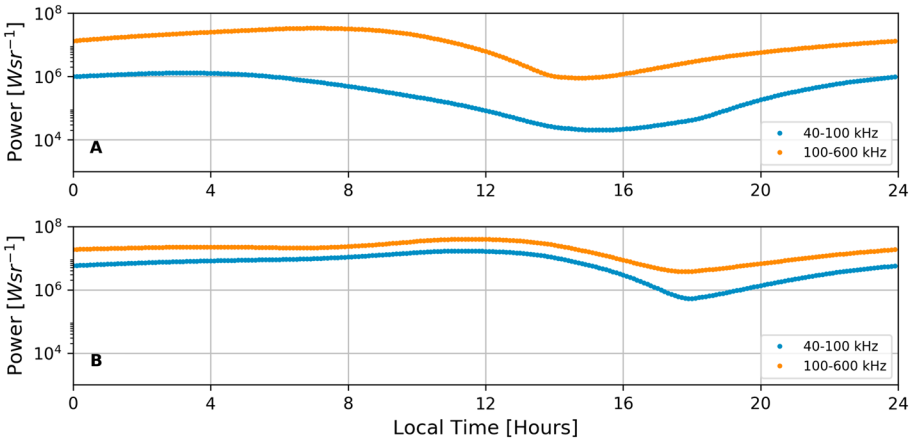

Figure 2. The integrated SKR power across two spectral ranges, 40–100 kHz (blue) and 100–600 kHz (orange) as a function of spacecraft local time. The 80th percentile of the 40–100 kHz spectral range and the 70th percentile of the 100–600 kHz spectral range is shown. (a) Low-latitude regions between −20° and 20°, and (b) latitudes greater than ±20°. The data were initially binned into 4 h local time bins and then interpolated to bins 0.1 h wide and then smoothed across 4 h.

As discussed in section 2, during 2006 Cassini explored a range of latitudes (−56° to +55°) and due to the differing SKR visibility we split our analysis into equatorial and higher latitudes to illustrate the different behavior. Figure 2 shows the variation of SKR power with local time over two spectral ranges from our data set, 40–100 kHz and 100–600 kHz as a function of spacecraft local time during 2006 for (a) latitudes between −20° and +20° and (b) latitudes greater than +20° or less than −20° for the 80 and 70th percentile, respectively. For each frequency range the received power is initially binned into local time bins 4 h wide. These bins are then interpolated to 0.1 h bin sizes and smoothed over a 4 h window to give a smooth curve (colored lines in Figure 2). This gives a power threshold for each local time section 0.1 h wide that the power must exceed. Results from comparison with a training set matched with a desire for statistical significance gave the final thresholds as the 80th percentile for the 40–100 kHz spectral range and the 70th percentile for the 100–600 kHz spectral range.

A key benefit of this approach is to achieve a smooth development of the automated criteria to avoid large sharp threshold jumps as the spacecraft moves between adjacent local time sectors. Due to the trajectory of the spacecraft there is no time spent by the spacecraft at local times 2–3 h and 14–15 h for latitudes greater than ±20° despite a threshold being shown at these local times. The threshold shown at these local times has been interpolated across the data gaps but will not be applied to any data.

To summarize, our criteria for selecting LFEs are as follows:

1. The integrated power in the 100–600 kHz frequency band must be greater than the local time-dependent 70th percentile for each latitude range.
2. The integrated power in the 40–100 kHz frequency band must be greater than the local time-dependent 80th percentile for each latitude range.

3.2. Clustering

The LFE algorithm returns each time step in the RPWS data set that matches the criteria as defined above. This gave 37,077 points across 2006 that satisfied the criteria. In practice, the SKR displays intensifications and LFEs on much longer time scales than the 90 s cadence of the data set, and thus, we applied a simple clustering algorithm to gather the points which fulfil the LFE criteria into local groups which represent distinct LFEs as shown in Figure 3. The "maximum gap size," defined below as 200 min, was again empirically tuned to give the best agreement with our by-eye training set. The clustering works as follows:

1. First point, i_1, is put into Cluster 1.
2. If at second point, i_2, $i_2 - i_1 \leq X$, where X is the maximum gap size = 200 min, i_2 is put into Cluster 1.
3. Else if $i_2 - i_1 > X$, a new cluster is started, and i_2 is put into that.
4. Continue for all points.

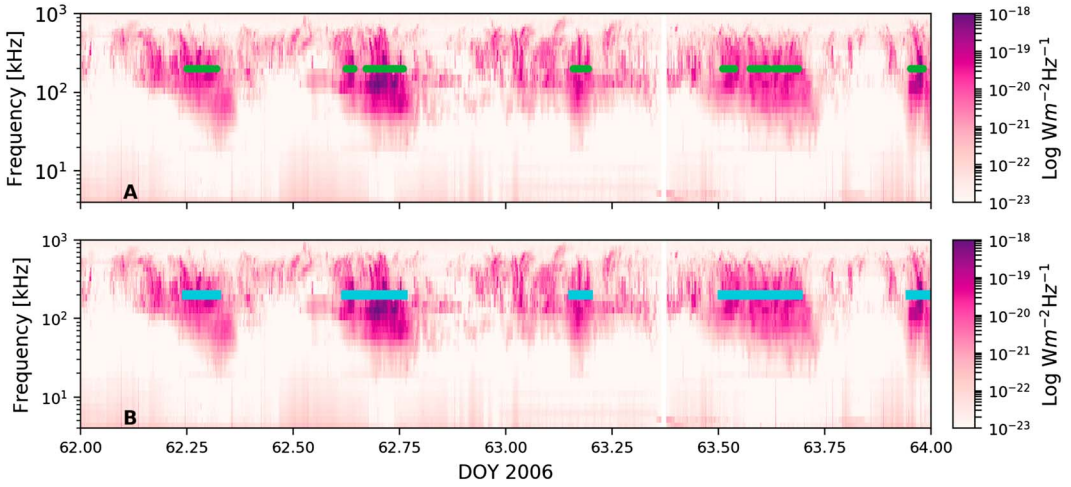

Figure 3. Example of LFE point clustering on a 2 day period between DOY 62 and 64 2006. (a) The 258 points (green circles) that satisfy the LFE criteria. (b) Those points clustered into five distinct LFEs (cyan rectangles).

Following the clustering of the points that meet the LFE criteria, we inspected the catalogue and removed those shorter than 30 min to ensure we were selecting sustained LFE events. On further examination of the entire catalogue, it became apparent that our LFE detection criteria select intense short events (such as those shown in Figure 3) well but do not select longer duration events that, while intense, are not continuously "extended," as successfully. These longer duration events are variable in intensity throughout and therefore can be split into multiple events by our algorithm when they are in fact a single event.

To account for this, we "join" shorter events based on the intensity of the power between them. For all events within 2 Saturn rotation periods (1 rotation taken here as 10.7 h) of the previous event, if more than 50% of the intervening time steps exceed the 60th percentile in the 100–600 kHz spectral range, we join these two events into one event. Figure 4 shows an example of this joining. The two cyan events in Figure 4a are selected individually by the LFE criteria described above. They are then joined together to form the yellow event shown in Figure 4b due to the SKR remaining significantly enhanced between them. Several further criteria are then applied to ensure we are selecting sustained low-frequency extensions. We remove events that start or end with a data gap or those with a large data gap within them. We also remove several events around spacecraft

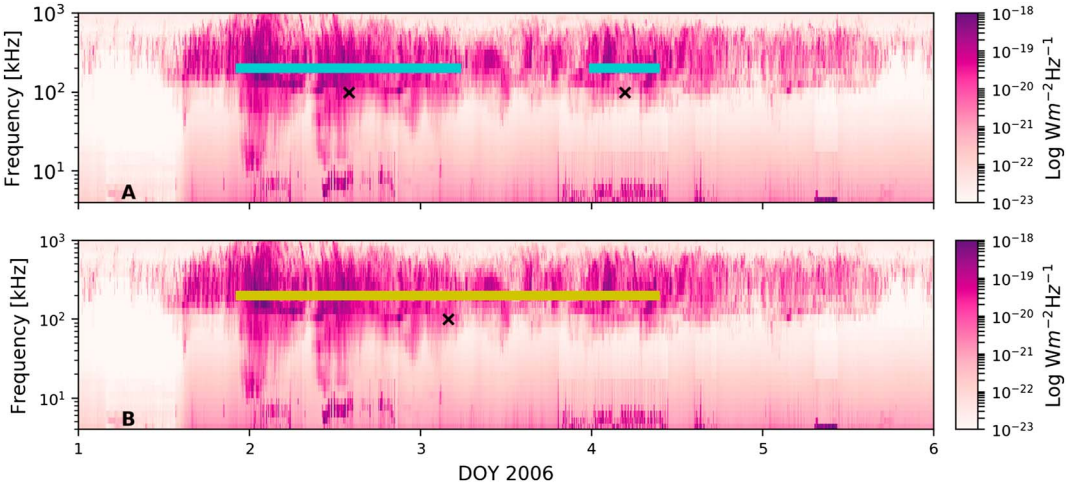

Figure 4. An example of the application of the "joining" criteria as discussed in the text. This shows 5 days of SKR data from DOY 1–6. (a) The "LFEs" that were detected by the original criteria and (b) the "new" LFEs as a result of the joining criteria. By eye it is clear that the SKR remains intense between the original LFEs (particularly when compared to the events shown in Figure 3 and that the whole feature has a different morphology to the events shown in Figure 3.

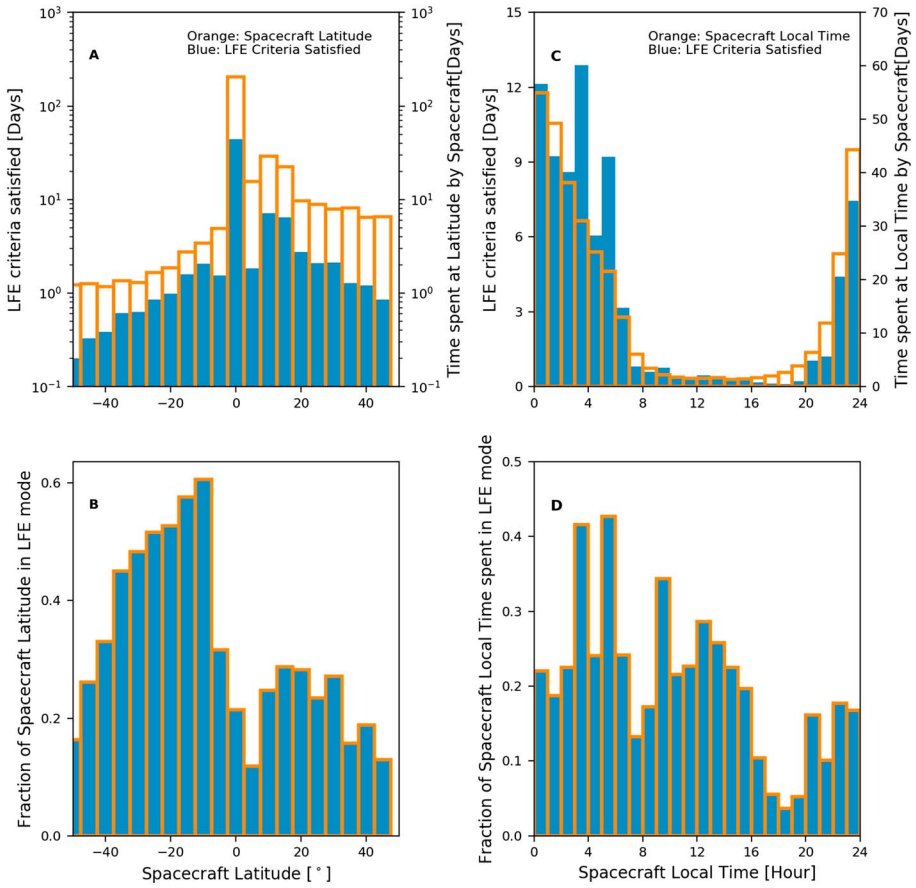

Figure 5. Distribution of LFEs as a function of (a and b) spacecraft latitude and (c and d) local time. Figure 5a shows the number of days within each spacecraft latitude that satisfied the LFE criteria (blue) and the distribution of spacecraft days at each latitude (orange outline). Figure 5b shows the fraction of the time the spacecraft spent at each latitude that satisfied the LFE criteria (blue and orange outline). The bin sizes are 5° latitude. There is a log scale in Figure 5a for both *y* axes emphasizing how many more events are seen at equatorial latitudes and how much more time the spacecraft spent there. Figure 5c shows the number of days within each spacecraft local time that satisfied the LFE criteria (blue) and the distribution of spacecraft days at each local time (orange outline). Figure 5d shows the fraction of the time the spacecraft spent at each local time that satisfied the LFE criteria (blue and orange outline). The bin sizes are 1 h of local time.

periapsis when the combination of spacecraft velocity and viewing conditions mean we cannot be confident that we are detecting an LFE from the spectrum. Following the application of these criteria, we find 282 LFEs for all of 2006.

4. Properties of LFEs

Now we have a final list of LFEs we begin to investigate their properties. In this section we will look at some of the properties of the LFE catalogue and what this can tell us about their role within the magnetosphere of Saturn. We first consider the distribution of LFEs detected across spacecraft local time and latitude.

4.1. LFE Viewing

Figure 5 shows the latitude spread of spacecraft trajectory and LFE observations, directly compared (Figure 5a) and normalized to time spent by the spacecraft at that latitude (Figure 5b). Similarly, Figures 5c and 5d show the local time spread of spacecraft trajectory and LFE observation, directly compared (Figure 5c) and normalized to time spent at that local time (Figure 5d). We take the spacecraft latitude and local time for all points throughout each LFE. When normalized to time spent at the local time, LFEs are observed fairly evenly across most local times with a peak in the early morning sector and a small dip in the predusk sector. This dip comes in the same local time region where the lowest SKR power is seen as shown in Figure 2. This may suggest that our location-dependent criteria do not sufficiently account for the variation in viewing. It should be noted that very little time is spent by the spacecraft at local times between ~10 and 19 h LT, and so the fraction in sectors

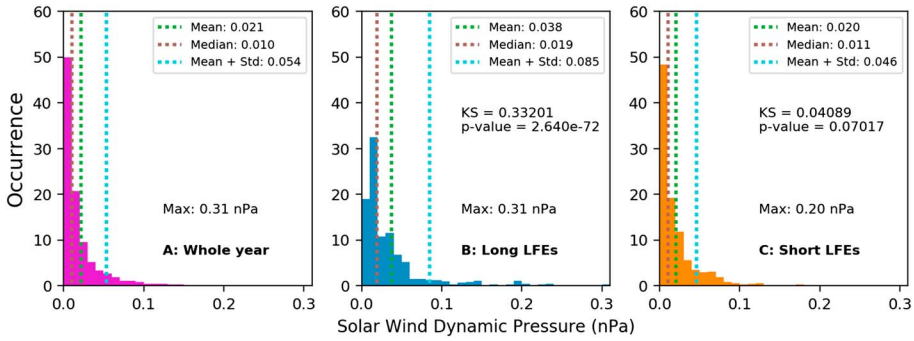

Figure 6. Comparing the average solar wind dynamic pressure during the (a) whole of 2006, (b) long LFEs >20 h, and (c) short LFEs <20 h. The mean (green), median (brown), and mean plus 1 standard deviation (cyan) is plotted on each figure. The maximum dynamic pressure in the distribution is also marked on each panel. Figures 6b and 6c show the results of two KS statistical tests comparing the average solar wind behavior across the whole year (Figure 6a) to the respective LFE type.

outside of this region is likely a better representation of LFE viewing. Not many LFEs are observed at equatorial latitudes as a fraction of time spent there and there are almost twice as many observed in the southern hemisphere than the northern. As with the local time distribution, the time spent at certain latitudes by the spacecraft is important. It should therefore be noted that 58% of 2006 was spent between $\pm 1°$ and so the fraction in this region is most likely a better representation of LFE viewing than, for example, for all latitudes greater than $\pm 30°$ which only make up 11% in total of 2006.

For the use of the SKR as a proxy for magnetospheric dynamics, these results are promising. There is good LFE detection at all local times and latitudes. Comparing to in situ algorithms for detecting reconnection events, we note that the S16 study only used data when Cassini was on the nightside (18–06 h) of the planet whereas we observe LFEs while the spacecraft is outside this sector, at local times between 6 and 11 h. We also observe LFEs while Cassini is in the sheath. As such we are potentially observing magnetospheric dynamics that would otherwise be missed. LFEs thus have the advantage over in situ (field and plasma) measurements that they are visible from most spacecraft locations and thus have potential to be used as a remote proxy for magnetospheric dynamics. In order to explore the degree to which they can be used a remote proxy, we will (in subsequent paper sections) test their relationships to various tail reconnection and solar wind dynamic pressure. This can then inform the degree of confidence with which we can use LFEs as a proxy for magnetospheric dynamics.

4.2. LFE Event Classification

We expect to see two types of LFE: "long" events replaced possibly associated with solar wind dynamics (Bunce et al., 2005, 2010; Clarke et al., 2009; Desch & Rucker, 1983; Kurth et al., 2005, 2016) and are usually longer than one planetary rotation, and also "short" events that have been associated with other phenomena such as tail reconnection (Jackman, Lamy, et al., 2009; Lamy et al., 2013) and are on the order of a few hours long. In order to differentiate between the two we select a threshold split time. Events shorter than this time are classified as short, while those longer are classified as long. We investigated the average behavior of the solar wind dynamic pressure during a selection of long and short LFEs for a range of split times and the behavior across 2006 as a whole. Based on this we selected a threshold time of 20 h which appeared to give the best by-eye and statistical separation of the different LFE types. Figure 6 shows the average solar wind behavior during the whole year (Figure 6a), long LFEs (Figure 6b), and short LFEs (Figure 6c).

The distribution of solar wind dynamic pressure during long LFEs had a mean and a median approximately twice that of the distribution for during short LFEs and versus the year as a whole and a maximum dynamic pressure 50% larger. We then performed a series of Kolmogorov-Smirnov (KS) statistical tests comparing the average solar wind behavior during 2006 as a whole, long LFEs, and short LFEs. Comparing the whole year and long LFEs gave a KS statistic of 0.33 and a p value $< 10^{-70}$ which suggests the average behavior is very different between the two. Next, comparing the whole year and the short LFEs gave a KS statistic of 0.04 and a p value of 0.07. While this p value is low (likely due to the long tail found in the whole year distribution with a skewness of 3.6 compared to 2.6 for the short LFEs), overall, this suggests that the two average behaviors are not too different. We then further compared the average solar wind behavior during the short and long LFEs

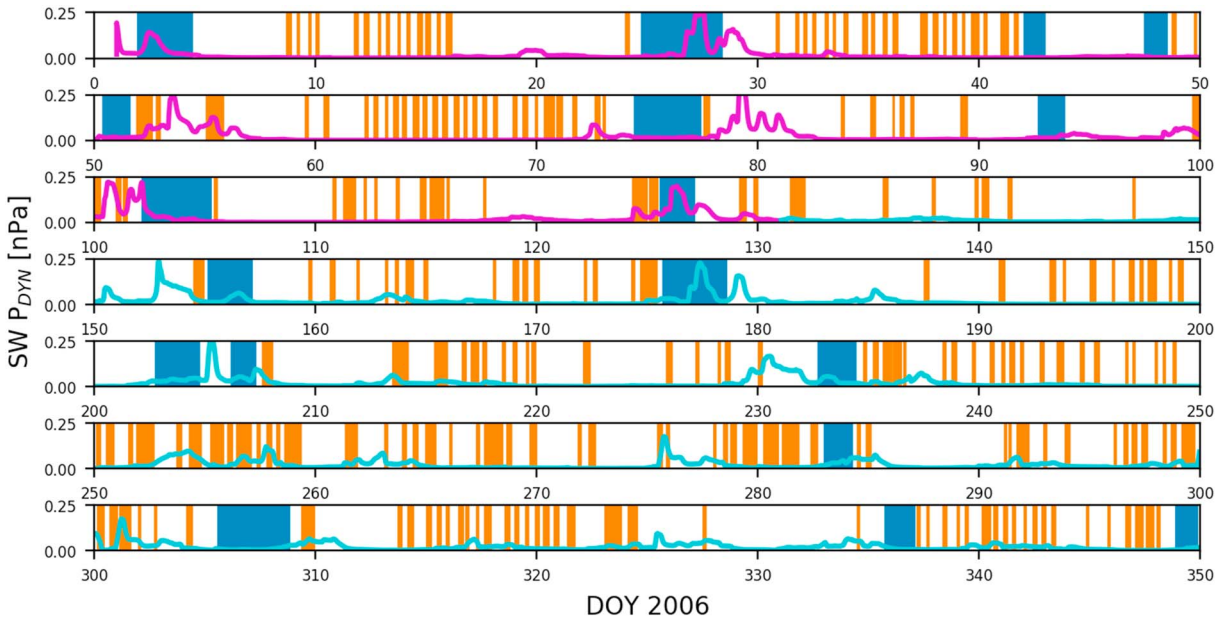

Figure 7. Comparing solar wind dynamic pressure (purple and cyan) as a function of time with long solar wind-driven events (blue) and shorter non–solar wind-driven events (orange). There are a total of 282 LFEs, 264 of which are short and 18 that are long. Solar wind dynamic pressure calculated within 75 days of apparent opposition is plotted in purple while that calculated further than 75 days is in cyan.

which gave a KS statistic of 0.31 and a p value of $< 10^{-40}$, which means we can conclude that the two groups are very likely not sampled from the same overriding distribution, that is, the solar wind is much different during one set of LFEs to the other.

Figure 7 shows the longer (blue) and shorter (orange) LFEs plotted against solar wind dynamic pressure as given by the mSWiM propagation model during 2006 for a split time between short and long LFEs of 20 h. The closest point of apparent opposition, where mSWiM propagation is most accurate, for 2006 is day of year 56. Within 75 days of this period (purple in Figure 7) we assume an error on mSWiM of $< \pm 20$ h, while we assume that the error is greater than this (up to 50 h) for periods further than 75 days (cyan in Figure 7) from apparent opposition. The 2006 was also at the minimum of solar cycle 23 and as such there are fewer transient events such as interplanetary coronal mass ejections meaning that mSWiM is particularly accurate. We will now investigate these two classifications further in sections 5 and 6.

5. Long LFEs

In this section we examine further the events that may be associated with solar wind dynamics as per the blue shaded regions in Figure 7. We examine their temporal properties and their relationship with phase.

5.1. Long LFEs: Temporal Properties

The solar wind movement away from the Sun is highly time and space dependent. The rotation of the Sun with a period, $P_{\mathrm{Rot}} \approx 25$ days as seen by Saturn, results in the interaction of solar wind streams of different speeds. This leads to two types of fronts: compression regions as high-speed solar wind pushes against slower moving plasma ahead and rarefactions where high-speed streams pull away from slower moving plasma behind (Parker et al., 1964). These features last longer than a solar rotation and so sweep past the planet at a periodicity of ~25 days as corotating interaction regions (CIRs). Jackman et al. (2004) examined Cassini measurements of the interplanetary magnetic field (IMF) during Saturn approach. They found that the IMF during this period was highly modulated during each solar rotation by CIR-related compressions lasting approximately 5 days, and longer rarefaction regions typically lasting around 7 days. As mentioned, 2006 was at the minimum of solar cycle 23 and so we would expect a well-structured two-sector (two alternating compression region/rarefaction regions) solar wind which would give a period of ~13 days. Hanlon et al. (2004) investigated the evolution of the solar wind between 1 and 5 AU (the orbit of Jupiter) and found that two compression regions at the orbit of Earth had merged into one by the time that they reached the orbit of Jupiter. As such,

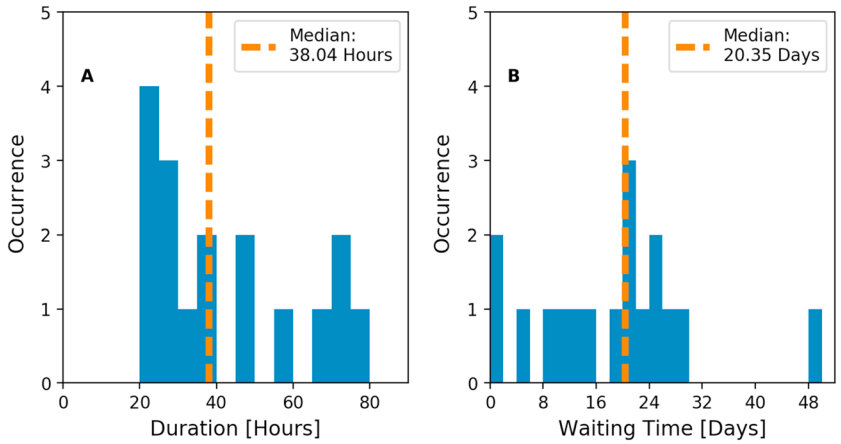

Figure 8. Solar wind-associated (a) LFE durations in hours and (b) waiting time in days. The median is marked by the orange line. There are a total of 18 solar wind-associated LFEs and 17 waiting times between consecutive events

we might expect a period of ~25 days which was also seen by Kurth et al. (2016). We now look at the properties of our long LFEs to see if they are consistent with these phenomena.

Figure 8 shows the distribution of long LFE durations (Figure 8a) and waiting times (Figure 8b). There is a wide range of event lengths with only a slight peak between 20 and 30 h, highlighting the variable nature of these events which is consistent with the time and spatial variability of the CIRs. The long LFEs can last for many planetary rotations. Four events have a waiting time of less than 10 days, less than either of the periodicities we might expect, although two of these can be accounted for by multiple large LFEs during periods of increased solar wind dynamic pressure. The 50% of the LFEs have a periodicity of between 18 and 30 days. This is within the region of time that we might expect if these longer events were associated with the dynamics of the solar wind with one compression per solar cycle. One event had a waiting time of approximately 48 days (~$2P_{Rot}$), which suggests we missed an event within a cycle (around DOY 255 in Figure 7).

5.2. Long LFEs: SKR Phase

We next look at the relationship of the long LFEs events to SKR phase. If the long LFE events are associated with the solar wind then we would expect no relationship between the timing of these events and the phase of the SKR since the solar wind behavior is independent of the rotation of Saturn. Figure 9 shows the northern and southern system SKR phases at the onset time of the long LFEs. There is no clear clustering of the LFEs at a particular phase, although there are only 18 events and so a relationship may become clearer with more events, although we think this is unlikely. These events last several planetary rotations, and thus, the phase of the planet can go through multiple cycles. In light of this we also check the phase relationship for the phase taken at the center of the event and find that there is still no clear relationship.

We note that we do observe a dependence on phase within the long LFEs. During these LFEs that last several planetary rotations, there are multiple intensifications of the SKR and multiple extensions down to lower frequencies. These very often coincide with the peak in the SKR phase suggesting there is still some underlying rotational component during these times (not shown).

6. Short LFEs

We next look at the shorter events from our LFE catalogue. By eye in Figure 7 it seems that these events do not typically correlate with increases in solar wind dynamic pressure. We examined this further by comparing the solar wind dynamic pressure behavior during these short LFEs against the behavior across all of 2006. We found that the mean and median of these distributions are essentially equal and a KS-test comparing the two distributions would suggest that they are very similar. From this we conclude that there is no significant change in solar wind dynamic pressure during short LFEs to non-LFE times and therefore that the short LFEs have no solar wind dependence. In this section and section 7 we investigate the drivers behind these events, their association with phase, and how well they correlate with tail reconnection events. We first look at their temporal properties.

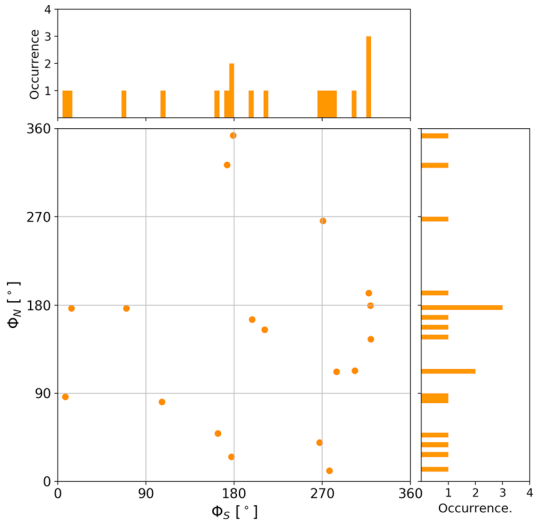

Figure 9. Scatterplots of long LFEs occurrence with the southern and northern SKR phase. The phase is taken at the start point of the LFE as defined by our criteria. The histograms show the distributions of the scattered points.

6.1. Short LFEs: Temporal Properties

Figure 10 shows the distribution of LFE duration for the short LFE events (those less than 20 h) in Figure 10a and the waiting times between successive short LFE events in Figure 10b. If these short events were associated with the rotational dynamics of the planet, either through SKR phase and current intensification or tail reconnection we would expect these events to have a duration of less than one planetary rotation and a waiting time on the order of one planetary rotation. We find that 233/264 events are less than 8 h long with a median for the entire set of 3.1 h. As expected this is much less than one planetary rotation. We note that these length values are only indicative as their value directly depends on the selection criteria. We also mention our minimum length criterion removed all events shorter than 30 min and as such the shortest event we observe can be a minimum of 30 min.

The median waiting time is ~10 h and there is a long tail with a few waiting times over a week long. If these LFEs were dependent on just the rotation of the planet, with ideal viewing conditions we might expect a waiting time of order ~10.7 h. In this case 63% of our events have a waiting time of less than 11 h which suggests that this periodicity does exist in some cases. As discussed in section 3 on criteria above, there is a large location dependency on the visibility of the SKR and so we are unlikely to be seeing all events which will affect our statistics.

As an additional note, we look at two specific 10 day periods (DOY 30–40 and 60–70) where the spacecraft has a good consistent viewing as it passes slowly through 4–5.1 h LT and 2–4 h LT, respectively, on an equatorial orbit. We find that 35 LFEs are detected in this period with a median waiting time between 8 and 9 h and a median length between 2.5 and 3 h. This gives a median cycle length of 10 to 12 h. This is consistent with our picture of these events being associated with the rotation of Saturn with period ~10.7 h.

6.2. Short LFEs: SKR Phase

We next look at the relationship of these short events with SKR phase. If they are related to the rotation of the planet we would expect to see a relationship between their start time with the SKR phase. The 2006 was southern hemisphere summer, and so the current sheet was hinged up out of the equatorial plane. For the first 205 days of 2006, Cassini was in low-latitude equatorial orbits, so spent most of the time in the southern hemisphere and therefore had best viewing conditions for the southern SKR source. Due to this, any phase relationship would be expected to be strongest with the southern SKR phase. Post day of year 205 Cassini moved to higher-latitude orbits and so saw both the northern and southern SKR sources were seen equally.

Figure 11 shows the northern and southern system SKR phases at the onset time of the short LFEs. Most of the events (149 out of 264) appear in the rising phase (where the SKR is increasing in power between 180° and the peak 0/360°) of both SKR systems (the upper right quadrant of Figure 11). The events are mostly grouped into

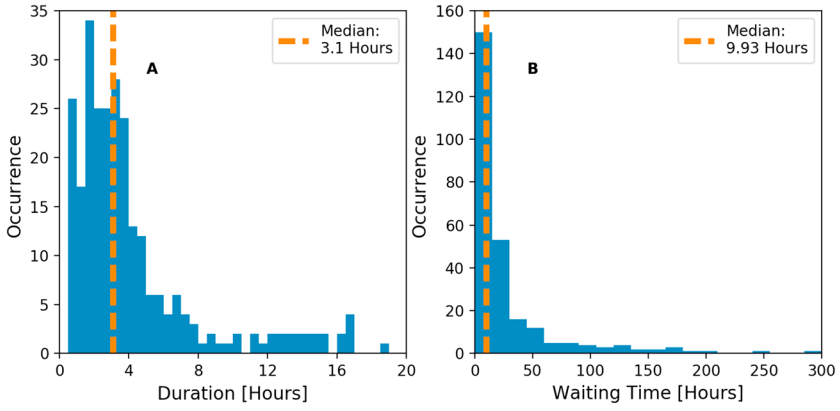

Figure 10. (a) Short LFE durations in hours and (b) waiting time in hours. The median is marked by the orange line. There are a total of 264 non–solar wind-associated short LFEs and 263 waiting times between consecutive events.

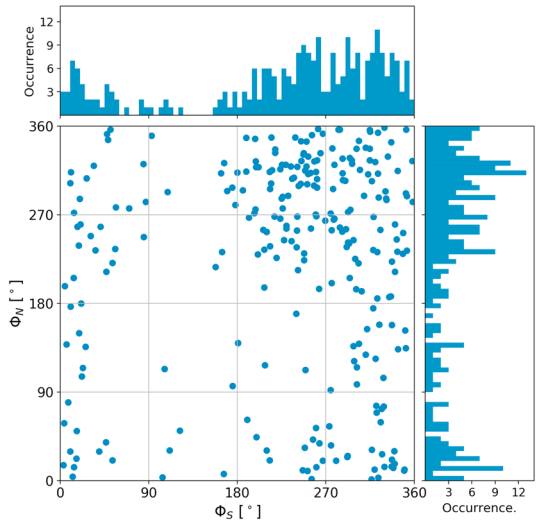

Figure 11. Scatterplots of non–solar wind-associated short LFEs occurrence on the southern and northern SKR phase. There are a total of 264 LFEs. The phase is taken at the start point of the LFE as defined by our criteria. The histograms show the distributions of the scattered points. The 149 of the 264 events can be found in the upper right quadrant where the northern and southern SKR phases are greater than 180°.

where the northern and southern systems are close to being in phase with each other around 270° southern SKR phase and 270° northern SKR phase. We examined further to explore if the clustering we see in this figure could happen by chance. We randomly selected 264 points in time in 2006 and noted their respective northern and southern phase values and recorded what fraction were in the same upper right quadrant as our actual data in Figure 11. We then repeated this 10,000 times. The mean percentage of points found in the upper right quadrant was 24.9% with a standard deviation of 2.7%, whereas 56.4% of our events are found in this quadrant (see supporting information Figure S1). It is therefore highly unlikely that we see this clustering by chance. If rotationally driven, nightside events need to rotate toward the dawn sector to match the expected SKR burst. Hence, considering the phase of the center point of the LFEs, we would expect the phases to cluster around 0/360°. As shown in Figure 12, we do see greater clustering at these points but there are still a few examples of the center points being completely out of phase with the SKR burst. We found that the clustering around periods where the systems were approximately in phase remained.

From our analysis we can see that there is a good relationship between these short LFEs and the phase of the SKR. As discussed in section 1, Jackman et al. (2016) found that there was a dependence on tail reconnection events with the magnetic phase (Andrews et al., 2011; Provan et al., 2011). The reconnection events used by Jackman et al. (2016) are those found by Jackman et al. (2014), a separate study to S16, although we do note that 90% of the events found by Jackman et al. (2014) were also found by the S16 study. Jackman et al. (2016) found that their reconnection events were clustered around 90° southern magnetic phase and 270° northern magnetic phase (although the northern SKR phase was used in lieu of the northern magnetic phase). As noted in section 1, this relative phase is associated with outward movement of plasma and a thin current sheet, ideal conditions for reconnection. During 2006, the southern magnetic and southern SKR phase were in antiphase (separated by 180°) (Andrews et al., 2012). The difference between the observed SKR and magnetic phase is a function of the spacecraft viewing conditions. During 2006, Cassini's orbit meant an approximately constant phase difference of 180° (Andrews et al., 2011) was observed. So with this in mind there is good agreement between the phases of the reconnection events and the short LFEs we have detected since the Jackman et al. (2016) events are clustered at 270° in northern and southern SKR phase, just like our short LFEs. In the next section we will look further at the relationshipbetween the LFEs and a known catalogue of reconnection events to try to establish how useful LFEs are as a proxy for reconnection in the tail.

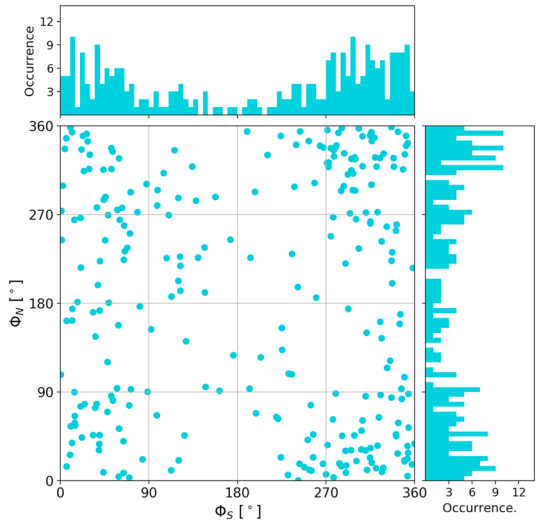

Figure 12. Scatterplots of non–solar wind-associated short LFEs occurrence with the southern and northern SKR phase. There are a total of 264 LFEs. The phase is taken at the center point of the LFE as defined by our criteria. The histograms show the distributions of the scattered points.

7. LFEs and Magnetospheric Dynamics

In this section we look further at the correlation between our LFE catalogue and tail reconnection events. As discussed in section 6, both LFEs and reconnection events occur preferentially at a particular phase of the planet's rotation. In order to assess the use of LFEs as a proxy for tail reconnection we examine the relationship in two ways: first checking how many LFEs have an associated reconnection event and second how many tail reconnection events have an associated LFE.

7.1. Comparison With Tail Reconnection Events

For comparison of LFEs to tail reconnection we need to ensure that we are only using LFEs detected while the spacecraft was in a favorable position for detecting reconnection events in situ. The S16 criteria required that the spacecraft was on the nightside of the planet (18–06 h LT), farther than 15 R_S, not in the magnetosheath and finally before DOY 282 in 2006. We removed LFEs that were detected when the spacecraft did not meet these

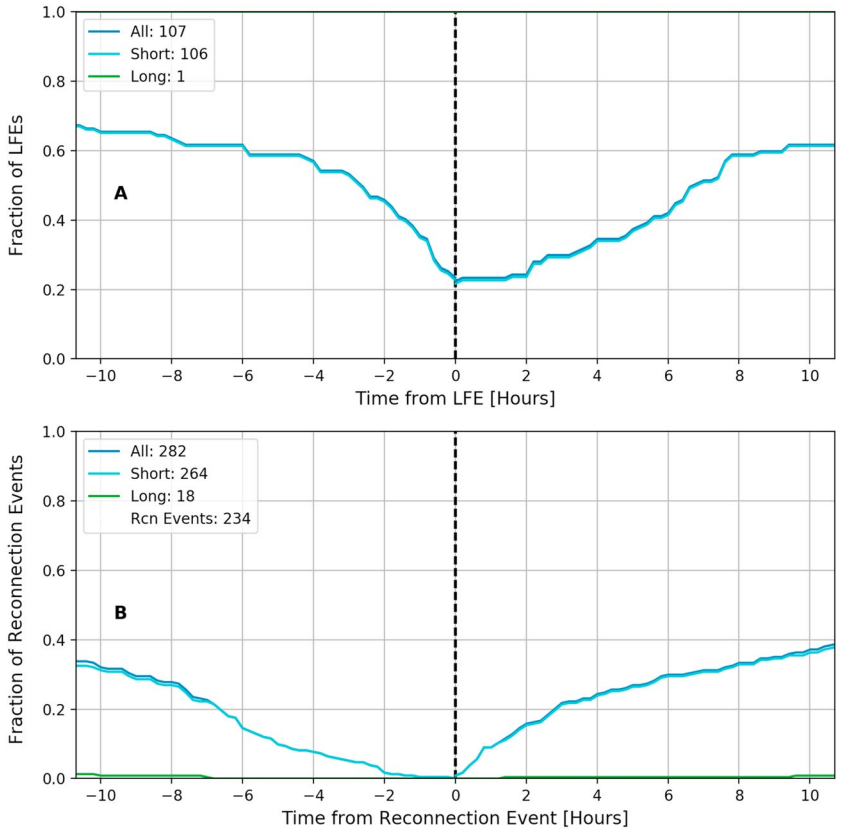

Figure 13. (a) The fraction of LFEs with an associated reconnection event as function of time before and after the LFE. Only LFEs that are detected while the spacecraft is in the reconnection event viewing region as defined by S16 are used. The *y* axis shows the fraction of the corresponding set of LFEs (all (blue), short (cyan), or long (green)) that have an associated reconnection event either simultaneously or within the window of time. The *x* axis gives the window of time in hours either side of the LFE where a reconnection event is looked for. (b) The inverse relationship, the fraction of reconnection events with an associated LFE as function of time before and after the reconnection event. Here all LFEs and reconnection events are used unlike when searching for reconnection events associated with an LFE. The *y* axis shows the fraction or reconnection events that have an LFE (grouped into all (blue), short (cyan), or long (green)) within the window of time. The *x* axis gives the window of time in hours either side of the reconnection event where a LFE is looked for.

criteria and those that occurred less than 11 h before leaving this viewing region. This gave 107 LFEs from our initial catalogue of 282 LFEs. For each LFE we checked whether a reconnection event occurred simultaneously or within a given window size before the start or after the end. We then performed the same search for our 234 reconnection events, checking before and after the event for LFEs. For this second analysis we used our complete list of 282 LFEs. For each analysis we split the LFEs into three categories. All short (<20 h) and long (>20 h). The numbers in each set for each analysis can be found in Figure 13.

Figure 13 shows the results of these comparisons. Figure 13a shows the fraction of LFEs that have an associated reconnection event within a specific window size. Figure 13b shows the fraction of reconnection events that have a LFE within a specific window size. As would be expected, increasing the search window size increases the number of corresponding events found. Approximately 23% of the short LFEs have a simultaneous reconnection event, that is, a window size of zero. The 67% of short LFEs have a reconnection event during or within the preceding 10.7 h of their occurrence, and ~61% within 6 h where the graph approximately flattens. Only 40% of reconnection events have any LFE during or within 0.7 h before or after they occur. We do not perform the analysis for window sizes greater than 10.7 h as we expect that LFE events found after this length of time are unrelated to the reconnection event due to the periodic nature of the intensifications in the SKR. This correlation between reconnection events and subsequent radio response is perhaps lower than we might have expected given our understanding of the physical mechanism behind LFE driving (as outlined at Earth by, e.g., Morioka et al., 2007, 2012, and at Saturn by Jackman, Lamy, et al., 2009). In order to

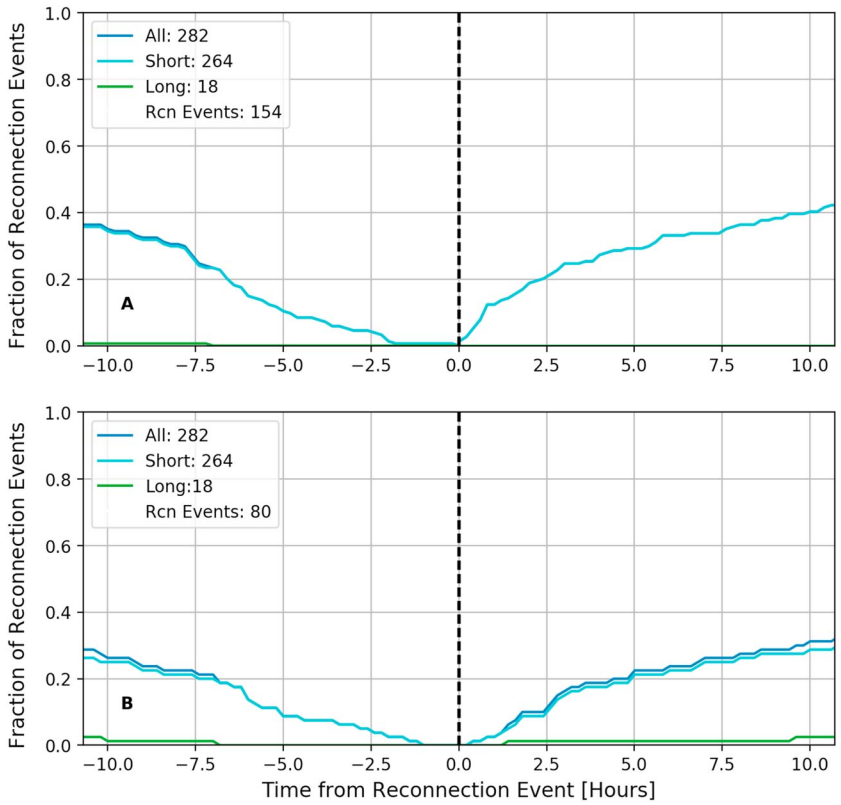

Figure 14. (a) Fraction of reconnection events detected in dawn sector with an associated LFE as a function of window size. (b) Fraction of reconnection events detected in the dusk sector with an associated LFE as a function of window size. Here all LFEs and reconnection events are used unlike when searching for reconnection events associated with an LFE. The two panels have a shared *x* axis.

investigate this further we did a significance check. During intervals that satisfied the viewing region criteria as defined by S16 we placed 106 short LFEs (with a distribution of lengths taken from Figure 10a) at various randomly selected start times. We then performed the same analysis as described above, seeing what fraction of those events had a reconnection event from the S16 catalogue in the preceding or following 6 h. We then repeated this 10,000 times. The mean number of LFEs with a reconnection event within the preceding 6 h was 39%. The 61% correlation we have is greater than 4 sigma confidence (see supporting information Figure S2). We do not comment on the relationship of the long LFEs to reconnection events since we have only 1 long events within the viewing region which is clearly not enough to be able to comment with any confidence. When finding reconnection events with associated long LFE events, the fraction is extremely low even for window sizes close to two planetary rotations. Overall, the fraction of reconnection events with an LFE is much lower than the inverse relationship, suggesting that while a LFE is a reasonable proxy that there has been reconnection in the tail, seeing a reconnection event in the tail does not always mean a reaction in the SKR will occur or be observed.

We further investigate the link between reconnection events and LFEs by examining the dependence of this relationship on spacecraft location. We separate the reconnection events into those detected at dusk ($n = 80$) and those in the dawn sector ($n = 154$) as seen in Figure 14. Due to the better SKR visibility in the dawn sector of the orbit closer to the strongest SKR source region around 8 h LT (Lamy et al., 2009), we might have expected a better "hit" rate for those detected while the spacecraft is in the dawn sector. There does not seem to be a difference in the fraction of reconnection events with an associated LFE between dusk and dawn. This suggests that our location-dependent criteria have accounted well for the variability in SKR visibility.

7.2. LFE Power

As shown and discussed above there is a reasonable correlation between short LFEs and tail reconnection (~60% of LFEs have a tail reconnection event simultaneously or within the preceding 6 h) and there is very strong correlation between the short LFEs start time and the northern and southern SKR phase systems.

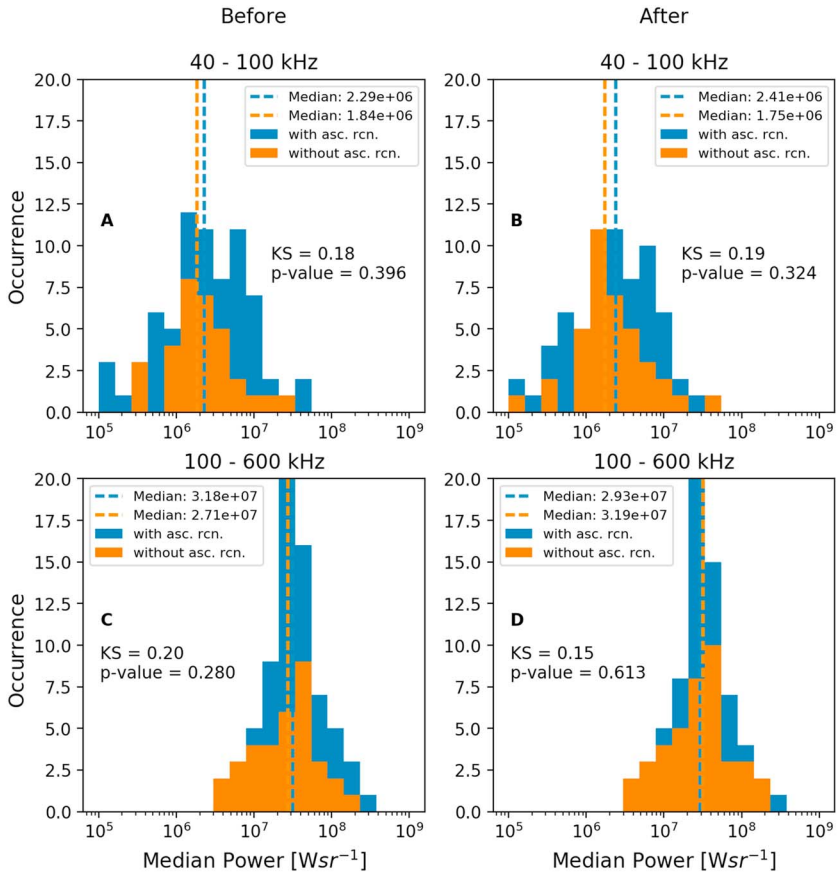

Figure 15. Histograms showing the distribution of median emitted powers of LFEs with (blue) or without (orange) an associated reconnection event within 6 h (a, c) before or (b, d) after the LFE in the two integrated power range: 40–100 kHz (Figures 15a and 15b) and 100–600 kHz (Figures 15c and 15d). The Kolmogorov-Smirnov statistic and *p* value are printed on each panel. Of the 106 short LFEs, there are 72 with an associated reconnection event within 6 h before and 66 after. There are 34 without an associated reconnection event within 6 h before and 40 after.

This phase in SKR system (when converted to magnetic phase) is also strongly associated with tail reconnection as shown in Jackman et al. (2016). This suggests a strong relationship between LFEs, tail reconnection, and the rotation of the planet. We next explore a potential explanation as to why the correlation between LFEs and tail reconnection is lower than we might expect.

There are two possible scenarios to explain this low correlation between LFEs and tail reconnection. (a) Not all LFEs are caused by tail reconnection or (b) the S16 catalogue that we are using to compare LFEs and reconnection events may be incomplete. During the above analysis, we attempted to limit this latter effect by limiting our LFEs to only those detected when the spacecraft was in a favorable position for detecting reconnection but it is likely that reconnection events (particularly small-scale events) were still missed. Reconnection detection, even within a favorable viewing region, is difficult. The size of the signature is a function of the trajectory of the spacecraft through the plasmoid or region as well as the orbit of the spacecraft considering the hinged current sheet that changes location with season. If (a), not all LFEs are caused by the increased precipitation of particles along fields due to tail reconnection, that suggests there are two or more drivers behind these shorter LFEs. To investigate this, we next compare the distribution of median emitted powers during short LFEs (<20 h) that do and do not have an associated reconnection event. A significantly differing distribution of powers between those LFEs driven by reconnection and those not driven by reconnection would allow us to better use LFEs as a proxy for magnetospheric dynamics by parametrizing the difference between the two types of short LFEs. If there is no difference in the distributions, this could suggest that in fact all of the LFEs are associated with reconnection and it is just that we have not observed the associated reconnection event in situ in the tail.

Figure 15 shows the median emitted power of the short LFEs ($n = 106$) seen in the S16 viewing region. The LFEs are separated into those with (blue) or without (orange) an associated reconnection event within 6 h before or after in two integrated frequency ranges: 40–100 kHz and 100–600 kHz. The Kolmogorov-Smirnov statistic and the p value comparing the two distributions on each panel is printed. These values show that we are unable to reject the null hypotheses that the two distributions have been drawn from the same distribution, that is, there is no statistical difference between the distribution of emitted power during LFEs with and without an associated reconnection event. Even varying the window size for searching for associated reconnection events does not improve the KS statistics. This suggests that there is no significant difference in intensity between LFEs caused by reconnection and those not. This could mean that the ∼61% correlation rate between LFEs and reconnection events (within 6 h) above is due to missed reconnection events rather than a lack thereof. Due to the limitations of a single spacecraft, reconnection events are still being missed despite being in the viewing region.

8. Discussion

In this study we have developed a criterion for the selection of LFEs of the Saturn Kilometric Radiation from processed RPWS data. The 282 LFEs were detected during 2006 based on these criteria. We then investigated the properties of the LFEs such as their duration and recurrence rate. Furthermore, we categorized these LFEs into two types short and long and investigated their relationship with SKR phase, solar wind dynamic pressure, and a catalogue of tail reconnection events.

On examination of our catalogue of events we found two categories of LFE. Shorter, single extension LFEs and longer, multiple extension LFEs. These two types of LFE were categorized based on their duration (less than or greater than 20 h) into short and long LFEs. The short LFEs were the most numerous and occurred most frequently. We found 264 of these events with a median recurrence time of ∼10 h compared to only 18 long events which had a median recurrence time of ∼20 days. The shorter events were predicted to be associated with the rotation of the planet and to therefore show a recurrence rate around 10.7 h. 63% of events have a waiting time of less than 11 h suggesting this periodicity does exist in many cases. The distribution of waiting times for the short LFEs is affected by events that we do not detect or select, reflected by the long tail in Figure 10b. While our criteria included a dependency on spacecraft observation location, it is still likely that there are missed emissions due to imperfect location-dependent criteria and poor SKR visibility or the beaming of the SKR due to a solar wind compression. Although in good viewing intervals like those discussed in section 6.1 (i.e., DOY 30–40) we do find a strong rotational modulation.

The strong SKR phase dependence of the short LFE events that are detected, where the LFE start times are strongly clustered during the rising (>180°) phase of the southern and northern SKR phase (149 out of 264 LFEs), does further imply a periodicity of the order of a planetary rotation and that the variation in the waiting time distribution is due to missed/nonselected events. The starting SKR phase of the LFE events matched well with the magnetic phase of the reconnection events in Jackman et al. (2016) when accounting for the 180° phase difference between the southern SKR and southern magnetic phase during 2006. These conditions being favorable for the outward displacement of plasma and a thin current sheet as discussed in sections 1 and 6.2. This result further strengthens the relationship between the rotation of the planet, reconnection, and LFE occurrence.

The 2006 was near the minimum phase of the last solar cycle where the solar wind is expected to be well structured and regular and so the waiting time of the long events was expected to reflect a pattern of compressions associated with corotating interaction regions in a two-sector solar wind with a recurrence pattern of approximately 25 days as seen by Kurth et al. (2016). We do see a clustering (50% of events) of recurrence times between 19 and 31 days (±6 days of expected). The median duration of these long events is ∼39 h, with several lasting more than 2 days (48 h), and so the 6 day window either side of the expected recurrence time allows for these durations since the recurrence time is calculated from the end of one event to the start of the next event. As discussed in section 5 we might also expect a 13 day periodicity to occur. We do see several events with this time scale waiting time, although we do note that some of these are events that occur within a single solar wind compression event. Work on the merging of CIR compression regions with increasing distance from the Sun may make it more likely for a given ∼25 day solar rotation to be dominated by one strong compression, which could lead to the increased importance of a 25 day repetition period over a 13 day one. Meredith et al. (2014) analyzed 12 auroral storms, representing significant brightening and poleward

expansion of the auroral oval, detected by the Hubble Space Telescope at Saturn, and associated with solar wind compression. They found a typical lifetime of ~16 h, significantly shorter than a solar wind-associated LFE.

The long LFE catalogue was also examined for correlation with SKR phase. Since most of them last multiple planetary rotations it is not obvious which point of the LFE to assign a phase to and so we checked the correlation between the SKR phase and the long LFE start and center times. Neither times showed any dependency on the SKR phase as would be expected if these events are dependent on solar wind dynamics rather than internally controlled. It is interesting to note that many of the long LFEs contain multiple intensifications and extensions to lower frequencies (not shown) which do show a dependency on SKR phase. This illustrates that while the solar wind can intensify the SKR above its typical level, the influence of rotational dynamics can also be superposed on this behavior. Based on their periodicities, the correlation of long LFEs with solar wind dynamic pressure as shown in Figure 7 and the morphology of these long LFE events, it would suggest that they are good proxies for solar wind dynamics.

One of the motivations behind this study was to assess how good LFEs are as a proxy for reconnection in the tail. How do LFEs and tail dynamics relate and can this help us overcome some of the issues of single spacecraft observations? In order to do this we compared our catalogue of LFEs to the S16 catalogue of tail reconnection events. We selected LFEs that were detected while the spacecraft was in a good location for detecting reconnection events as defined by S16. Of the 107 LFEs detected during this period, 61% of all LFEs had a reconnection event within ±6 h. We then examined the number of reconnection events with an associated LFE. Of the 234 reconnection events, less than 20% had a LFE within ±6 h. This suggested that while an LFE more than likely signified a reconnection event had occurred, a reconnection event does not necessarily lead to a LFE (or one being observed).

We looked for both a reconnection event within a given window before and after a LFE and a LFE within a given window before and after a reconnection event. The mechanism put forward by Jackman, Lamy, et al. (2009) is as follows: Following reconnection, there is an increased precipitation of particles along field lines into the auroral regions. This increases until the electron density is larger than the plasma can carry and a taller acceleration region is required. The top of this acceleration (which is now radially further from the planet) region may coincide with a SKR source region at correspondingly higher altitudes and thus a weaker field strength, and so the emission moves to lower frequencies. In this scenario we would expect the causal relationship to be reconnection followed by an LFE. One complication lies in the estimation of the reconnection time. We do not detect reconnection directly; instead, we detect its products in the form of a plasmoid, dipolarization or TCR, and therefore, estimates are required on both the reconnection time and location. Following reconnection, the energized particles must travel along the field line to the planet, the time taken being dependent on the distance of the reconnection site to the SKR source region. Looking at the LFE/reconnection event relationship further, we find that there are more LFEs with associated reconnection events before than after which can be explained by the Jackman, Lamy, et al. (2009) mechanism time line (reconnection followed by LFE).

There are a several factors that could account for a perhaps lower than expected correlation between LFEs and reconnection events. As discussed above, the visibility of the SKR varies with spacecraft location and so it is possible that an LFE did occur but was not seen despite the location dependency built into the LFE criteria. Another factor is the size of the reconnection event itself. There are a range of reconnection event sizes. As a first approximation to the size of a reconnection event we can look at the magnitude of the field deflection associated with events, ΔB_θ. While highly dependent on the trajectory of the spacecraft through the structure and this distance of the spacecraft from the magnetospheric current sheet the S16 catalogue observes $|\Delta B_\theta|$ between 0.25 and 4.7 nT, and we would expect there to be a similar variation in SKR response. At Earth, the global impact of tail reconnection might be quantified through examination of flux closure or change in auroral electrojet indices (Coxon et al., 2014; Milan et al., 2009). However, at Saturn we lack such clear definitive measures of "substorm" size. Future work at Saturn should focus on the examination of the degree to which remote proxies such as radio emissions can serve as proxies for reconnection, not just in terms of timing of events but also in terms of estimating their size/global influence.

Approximately 61% of LFEs seen within the reconnection viewing region as defined by S16 have a reconnection event during or within 6 h before. This hit rate is reasonable but perhaps not as strong as we would expect if LFEs were indeed a good proxy for reconnection. Despite this a significance test showed that it is highly unlikely that this correlation would appear by chance. Further, if we consider the factors discussed such as the

varying strength of the reconnection events, the reconnection events that may have been missed and also consider the very good agreement between the phase of the reconnection events in Jackman et al. (2016) and of our LFEs, it would suggest there is in fact a good correlation between reconnection and LFEs at Saturn and that LFEs are indeed a good proxy for tail reconnection within the magnetosphere.

In order to test the reliability of our conclusions we performed the same analyses presented above on a smaller catalogue of LFEs derived from different criteria. The criteria for this second LFE catalogue was still based on exceeding a spacecraft location-dependent threshold in the two integrated power bands but with the additional criterion requiring the flux intensity at a specific low frequency to exceed a threshold. This catalogue contained 188 LFEs, 169 of which are also found in the main criteria described above. The results were consistent with those described above both in the general properties of the short and long LFEs, that is, including duration, recurrence rate, and where they were observed; and in their relationship with SKR phase and tail reconnection. The second catalogue actually showed a better relationship with tail reconnection events (~75% had a reconnection event simultaneously or within the previous 6 h compared to 60% for the catalogue described above). We interpret this as the second criteria selecting more significant (greater intensity and/or extended) events which, with the caveat of viewing constraints, may be associated with larger tail reconnection events which are more likely to be observed in the tail.

9. Summary

In this study we have developed a criterion for the selection of low-frequency extensions of the Saturn Kilometric Radiation from processed RPWS data. The 282 LFEs were detected during 2006 based on these criteria. We then investigated the properties of the LFEs such as their duration and recurrence rate. We also investigated their relationship with solar wind dynamic pressure, a catalogue of tail reconnection events and the northern and southern SKR phase systems.

1. The 282 LFEs were detected during 2006.
2. Eighteen of these events were longer than 20 h and strongly associated with increased solar wind dynamic pressure and showed no SKR phase dependency.
3. Of the 264 events shorter than 20 h, 107 were detected during periods that satisfied tail reconnection viewing conditions. Of those events ~61% had a reconnection event within 6 h or during the LFE. The start of all the short LFEs showed a strong relationship with the rising phase of both the southern and northern SKR phase systems.
4. There was no significant difference in emitted power during LFEs that did and did not have a reconnection event within ±6 h which would have suggested a different driving mechanism. This suggests that the nonperfect correlation may be due to "missed" reconnection events.
5. Short LFEs are a good proxy for tail reconnection within the magnetosphere.

Acknowledgments
J. J. Reed is supported by EPSRC Doctoral Training grant (EP/G03690X/1). C. M. J. is supported by STFC Ernest Rutherford FellowshipST/L004399/1. SKR data were accessed through the Cassini/RPWS/HFR data server http://www.lesia.obspm.fr/kronos. This facility was developed at Observatory of Paris/LESIA thanks to the support of CNRS and CNES institutes. The research at the University of Iowa (W. S. Kurth) was supported by NASA through contract 1415150 with the Jet Propulsion Laboratory. D. K. Whiter was supported by NERC grant NE/N004051/1. J. J. Reed would like to thank A. W. Smith and J. A. Reidy for helpful discussion.

References

Andrews, D. J., Cecconi, B., Cowley, S. W. H., Dougherty, M. K., Lamy, L., Provan, G., & Zarka, P. (2011). Planetary period oscillations in Saturn's magnetosphere: Evidence in magnetic field phase data for rotational modulation of Saturn kilometric radiation emissions. *Journal of Geophysical Research*, *116*, A09206. https://doi.org/10.1029/2011JA016636

Andrews, D. J., Cowley, S. W. H., Dougherty, M. K., Lamy, L., Provan, G., & Southwood, D. J. (2012). Planetary period oscillations in Saturn's magnetosphere: Evolution of magnetic oscillation properties from southern summer to post-equinox. *Journal of Geophysical Research*, *117*, A04224. https://doi.org/10.1029/2011JA017444

Andrews, D. J., Cowley, S. W. H., Dougherty, M. K., & Provan, G. (2010). Magnetic field oscillations near the planetary period in Saturn's equatorial magnetosphere: Variation of amplitude and phase with radial distance and local time. *Journal of Geophysical Research*, *115*, A04212. https://doi.org/10.1029/2009JA014729

Badman, S. V., Cowley, S. W. H., Lamy, L., Cecconi, B., & Zarka, P. (2008). Relationship between solar wind corotating interaction regions and the phasing and intensity of Saturn kilometric radiation bursts. *Annales Geophysicae*, *26*(12), 3641–3651. https://doi.org/10.5194/angeo-26-3641-2008

Bunce, E. J., Cowley, S. W. H., Talboys, D. L., Dougherty, M. K., Lamy, L., Kurth, W. S., … Coates, A. J. (2010). Extraordinary field-aligned current signatures in Saturn's high-latitude magnetosphere: Analysis of Cassini data during Revolution 89. *Journal of Geophysical Research*, *115*, A10238. https://doi.org/10.1029/2010JA015612

Bunce, E. J., Cowley, S. W. H., Wright, D. M., Coates, A. J., Dougherty, M. K., Krupp, N., … Rymer, A. M. (2005). In situ observations of a solar wind compression-induced hot plasma injection in Saturn's tail. *Geophysical Research Letters*, *32*, L20S04. https://doi.org/10.1029/2005GL022888

Burch, J. L., DeJong, A. D., Goldstein, J., & Young, D. T. (2009). Periodicity in Saturn's magnetosphere: Plasma cam. *Geophysical Research Letters*, *36*, L14203. https://doi.org/10.1029/2009GL039043

Burch, J. L., Goldstein, J., Mokashi, P., Lewis, W. S., Paty, C., Young, D. T., … André, N. (2008). On the cause of Saturn's plasma periodicity. *Geophysical Research Letters*, *35*, L14105. https://doi.org/10.1029/2008GL034951

Cecconi, B., & Zarka, P. (2005). Model of a variable radio period for Saturn. *Journal of Geophysical Research*, *110*, A12203. https://doi.org/10.1029/2005JA011085

Clarke, J. T., Gérard, J.-C., Grodent, D., Wannawichian, S., Gustin, J., Connerney, J., … Kim, J. (2005). Morphological differences between Saturn's ultraviolet aurorae and those of Earth and Jupiter. *Nature*, *433*(7027), 717–719. https://doi.org/10.1038/nature03331

Clarke, J. T., Nichols, J., Gérard, J. C., Grodent, D., Hansen, K. C., Kurth, W., … Cecconi, B. (2009). Response of Jupiter's and Saturn's auroral activity to the solar wind. *Journal of Geophysical Research*, *114*, A05210. https://doi.org/10.1029/2008JA013694

Clarke, K. E., Andrews, D. J., Arridge, C. S., Coates, A. J., & Cowley, S. W. H. (2010). Magnetopause oscillations near the planetary period at Saturn: Occurrence, phase, and amplitude. *Journal of Geophysical Research*, *115*, A08209. https://doi.org/10.1029/2009JA014745

Clarke, K. E., Andrews, D. J., Coates, A. J., Cowley, S. W. H., & Masters, A. (2010). Magnetospheric period oscillations of Saturn's bow shock. *Journal of Geophysical Research*, *115*, A05202. https://doi.org/10.1029/2009JA015164

Cowley, S. W. H., Bunce, E. J., & O'Rourke, J. M. (2004). A simple quantitative model of plasma flows and currents in Saturn's polar ionosphere. *Journal of Geophysical Research*, *109*(A5), A05212. https://doi.org/10.1029/2003JA010375

Cowley, S. W., & Provan, G. (2016). Planetary period oscillations in Saturn's magnetosphere: Further comments on the relationship between post-equinox properties deduced from magnetic field and Saturn kilometric radiation measurements. *Icarus*, *272*, 258–276. https://doi.org/10.1016/j.icarus.2016.02.051

Coxon, J. C., Milan, S. E., Clausen, L. B., Anderson, B. J., & Korth, H. (2014). The magnitudes of the regions 1 and 2 Birkeland currents observed by AMPERE and their role in solar wind-magnetosphere-ionosphere coupling. *Journal of Geophysical Research: Space Physics*, *119*, 9804–9815. https://doi.org/10.1002/2014JA020138

Desch, M. D. (1982). Evidence for solar wind control of Saturn radio emission. *Journal of Geophysical Research*, *87*(A6), 4549. https://doi.org/10.1029/JA087iA06p04549

Desch, M. D., & Kaiser, M. L. (1981). Voyager measurement of the rotation period of Saturn's magnetic field. *Geophysical Research Letters*, *8*(3), 253–256. https://doi.org/10.1029/GL008i003p00253

Desch, M. D., & Rucker, H. O. (1983). The relationship between Saturn kilometric radiation and the solar wind. *Journal of Geophysical Research*, *88*(A11), 8999–9006. https://doi.org/10.1029/JA088iA11p08999

Dougherty, M. K. (2005). Cassini magnetometer observations during saturn orbit insertion. *Science*, *307*(5713), 1266–1270. https://doi.org/10.1126/science.1106098

Dougherty, M. K., Kellock, S., Southwood, D. J., Balogh, A., Smith, E. J., Tsurutani, B. T., … Cowley, S. W. H. (2004). The Cassini magnetic field investigation. *Space Science Reviews*, *114*(1–4), 331–383. https://doi.org/10.1007/s11214-004-1432-2

Fischer, G., Gurnett, D. A., Kurth, W. S., Ye, S. Y., & Groene, J. B. (2015). Saturn kilometric radiation periodicity after equinox. *Icarus*, *254*, 72–91. https://doi.org/10.1016/j.icarus.2015.03.014

Galopeau, P. H. M., & Lecacheux, A. (2000). Variations of Saturn's radio rotation period measured at kilometer wavelengths. *Journal of Geophysical Research*, *105*(A6), 13,089–13,101. https://doi.org/10.1029/1999JA005089

Gurnett, D. A. (2005). Radio and plasma wave observations at Saturn from Cassini's approach and first orbit. *Science*, *307*(5713), 1255–1259. https://doi.org/10.1126/science.1105356

Gurnett, D. A. (2011). An SLS4 longitude system based on a tracking filter analysis of the rotational modulation of Saturn kilometric radiation, *Planetary Radio Emissions Vii* (pp. 51–64). Vienna: Austrian Academy of Sciences Press. https://doi.org/10.1553/PRE7s51

Gurnett, D. A., Groene, J. B., Persoon, A. M., Menietti, J. D., Ye, S. Y., Kurth, W. S., … Lecacheux, A. (2010). The reversal of the rotational modulation rates of the north and south components of Saturn kilometric radiation near equinox. *Geophysical Research Letters*, *37*, L24101. https://doi.org/10.1029/2010GL045796

Gurnett, D. A., Kurth, W. S., Kirchner, D. L., Hospodarsky, G. B., Averkamp, T. F., Zarka, P., … Pedersen, A. (2004). The Cassini radio and plasma wave investigation. *Space Science Reviews*, *114*(1–4), 395–463. https://doi.org/10.1007/s11214-004-1434-0

Gurnett, D. A., Persoon, A. M., Groene, J. B., Kopf, A. J., Hospodarsky, G. B., & Kurth, W. S. (2009). A north-south difference in the rotation rate of auroral hiss at Saturn: Comparison to Saturn's kilometric radio emission. *Geophysical Research Letters*, *36*, L21108. https://doi.org/10.1029/2009GL040774

Gurnett, D. A., Persoon, A. M., Kurth, W. S., Groene, J. B., Averkamp, T. F., Dougherty, M. K., & Southwood, D. J. (2007). The variable rotation period of the inner region of Saturn's plasma disk. *Science*, *316*(5823), 442–445. https://doi.org/10.1126/science.1138562

Hanlon, P. G., Dougherty, M. K., Forsyth, R. J., Owens, M. J., Hansen, K. C., Tóth, G., … Young, D. T. (2004). On the evolution of the solar wind between 1 and 5 AU at the time of the Cassini Jupiter flyby: Multispacecraft observations of interplanetary coronal mass ejections including the formation of a merged interaction region. *Journal of Geophysical Research*, *109*, A09S03. https://doi.org/10.1029/2003JA010112

Hunt, G. J., Cowley, S. W. H., Provan, G., Bunce, E. J., Alexeev, I. I., Belenkaya, E. S., … Coates, A. J. (2014). Field-aligned currents in Saturn's southern nightside magnetosphere: Subcorotation and planetary period oscillation components. *Journal of Geophysical Research: Space Physics*, *119*, 9847–9899. https://doi.org/10.1002/2014JA020506

Hunt, G. J., Cowley, S. W. H., Provan, G., Bunce, E. J., Alexeev, I. I., Belenkaya, E. S., … Coates, A. J. (2015). Field-aligned currents in Saturn's northern nightside magnetosphere: Evidence for interhemispheric current flow associated with planetary period oscillations. *Journal of Geophysical Research: Space Physics*, *120*, 7552–7584. https://doi.org/10.1002/2015JA021454

Jackman, C. M., Achilleos, N., Bunce, E. J., Cowley, S. W. H., Dougherty, M. K., Jones, G. H., … Smith, E. J. (2004). Interplanetary magnetic field at ~9 AU during the declining phase of the solar cycle and its implications for Saturn's magnetospheric dynamics. *Journal of Geophysical Research*, *109*, A11203. https://doi.org/10.1029/2004JA010614

Jackman, C. M., Arridge, C. S., McAndrews, H. J., Henderson, M. G., & Wilson, R. J. (2009). Northward field excursions in Saturn's magnetotail and their relationship to magnetospheric periodicities. *Geophysical Research Letters*, *36*, L16101. https://doi.org/10.1029/2009GL039149

Jackman, C. M., Lamy, L., Freeman, M. P., Zarka, P., Cecconi, B., Kurth, W. S., … Dougherty, M. K. (2009). On the character and distribution of lower-frequency radio emissions at Saturn and their relationship to substorm-like events. *Journal of Geophysical Research*, *114*, A08211. https://doi.org/10.1029/2008JA013997

Jackman, C. M., Provan, G., & Cowley, S. W. (2016). Reconnection events in Saturn's magnetotail: Dependence of plasmoid occurrence on planetary period oscillation phase. *Journal of Geophysical Research: Space Physics*, *121*, 2922–2934. https://doi.org/10.1002/2015JA021985

Jackman, C. M., Slavin, J. A., Kivelson, M. G., Southwood, D. J., Achilleos, N., Thomsen, M. F., … Vogt, M. F. (2014). Saturn's dynamic magnetotail: A comprehensive magnetic field and plasma survey of plasmoids and traveling compression regions and their role in global magnetospheric dynamics. *Journal of Geophysical Research: Space Physics*, *119*, 5465–5494. https://doi.org/10.1002/2013JA019388

Kaiser, M. L., & Desch, M. D. (1984). Radio emissions from the planets Earth, Jupiter, and Saturn. *Reviews of Geophysics*, *22*, 373–384. https://doi.org/10.1029/RG022i004p00373

Kaiser, M. L., Desch, M. D., Warwick, J. W., & Pearce, J. B. (1980). Voyager detection of nonthermal radio emission from Saturn. *Science*, *209*(4462), 1238 LP–1240. https://doi.org/10.1126/science.209.4462.1238

Kennelly, T. J., Leisner, J. S., Hospodarsky, G. B., & Gurnett, D. A. (2013). Ordering of injection events within Saturnian SLS longitude and local time. *Journal of Geophysical Research: Space Physics*, *118*, 832–838. https://doi.org/10.1002/jgra.50152

Kimura, T., Lamy, L., Tao, C., Badman, S. V., Kasahara, S., Cecconi, B., … Fujimoto, M. (2013). Long-term modulations of Saturn's auroral radio emissions by the solar wind and seasonal variations controlled by the solar ultraviolet flux. *Journal of Geophysical Research: Space Physics*, *118*, 7019–7035. https://doi.org/10.1002/2013JA018833

Kurth, W. S., Averkamp, T. F., Gurnett, D. A., Groene, J. B., & Lecacheux, A. (2008). An update to a Saturnian longitude system based on kilometric radio emissions. *Journal of Geophysical Research*, *113*, A05222. https://doi.org/10.1029/2007JA012861

Kurth, W. S., Gurnett, D. A., Clarke, J. T., Zarka, P., Desch, M. D., Kaiser, M. L., … Crary, F. J. (2005). An Earth-like correspondence between Saturn's auroral features and radio emission. *Nature*, *433*(7027), 722–725. https://doi.org/10.1038/nature03334

Kurth, W. S., Hospodarsky, G. B., Gurnett, D. A., Lamy, L., Dougherty, M. K., Nichols, J., … Crary, F. J. (2016). Saturn kilometric radiation intensities during the Saturn auroral campaign of 2013. *Icarus*, *263*, 2–9. https://doi.org/10.1016/j.icarus.2015.01.003

Lamy, L. (2011). Variability of southern and northern periodicities of Saturn Kilometric Radiation, *Planetary Radio Emissions V11* (pp. 15–17). Vienna: Austrian Academy of Sciences press.

Lamy, L., Zarka, P., Cecconi, B., Prangé, R., Kurth, W. S., & Gurnett, D. A. (2008). Saturn kilometric radiation: Average and statistical properties. *Journal of Geophysical Research*, *113*, A07201. https://doi.org/10.1029/2007JA012900

Lamy, L., Cecconi, B., Prangé, R., Zarka, P., Nichols, J. D., & Clarke, J. T. (2009). An auroral oval at the footprint of Saturn's kilometric radio sources, colocated with the UV aurorae. *Journal of Geophysical Research*, *114*, A10212. https://doi.org/10.1029/2009JA014401

Lamy, L., Cecconi, B., Zarka, P., Canu, P., Schippers, P., Kurth, W. S., … Louarn, P. (2011). Emission and propagation of Saturn kilometric radiation: Magnetoionic modes, beaming pattern, and polarization state. *Journal of Geophysical Research*, *116*, A04212. https://doi.org/10.1029/2010JA016195

Lamy, L., Prangé, R., Pryor, W., Gustin, J., Badman, S. V., Melin, H., … Brandt, P. C. (2013). Multispectral simultaneous diagnosis of Saturn's aurorae throughout a planetary rotation. *Journal of Geophysical Research: Space Physics*, *118*, 4817–4843. https://doi.org/10.1002/jgra.50404

Lamy, L., Schippers, P., Zarka, P., Cecconi, B., Arridge, C. S., Dougherty, M. K., … Coates, A. J. (2010). Properties of Saturn kilometric radiation measured within its source region. *Geophysical Research Letters*, *37*, L12104. https://doi.org/10.1029/2010GL043415

Lamy, L., Zarka, P., Cecconi, B., & Prangé, R. (2010). Auroral kilometric radiation diurnal, semidiurnal, and shorter-term modulations disentangled by Cassini. *Journal of Geophysical Research*, *115*, A09221. https://doi.org/10.1029/2010JA015434

Louarn, P., Kurth, W. S., Gurnett, D. A., Hospodarsky, G. B., Persoon, A. M., Cecconi, B., … Blanc, M. (2007). Observation of similar radio signatures at Saturn and Jupiter: Implications for the magnetospheric dynamics. *Geophysical Research Letters*, *34*, L20113. https://doi.org/10.1029/2007GL030368

Menietti, J. D., Mutel, R. L., Schippers, P., Ye, S. Y., Gurnett, D. A., & Lamy, L. (2011). Analysis of Saturn kilometric radiation near a source center. *Journal of Geophysical Research*, *116*, A12222. https://doi.org/10.1029/2011JA017056

Meredith, C. J., Cowley, S. W. H., & Nichols, J. D. (2014). Survey of Saturn auroral storms observed by the Hubble Space Telescope: Implications for storm time scales. *Journal of Geophysical Research: Space Physics*, *19*, 9624–9642. https://doi.org/10.1002/2014JA020601

Milan, S. E., Grocott, A., Forsyth, C., Imber, S. M., Boakes, P. D., & Hubert, B. (2009). A superposed epoch analysis of auroral evolution during substorm growth, onset and recovery: Open magnetic flux control of substorm intensity. *Annales Geophysicae*, *27*(2), 659–668. https://doi.org/10.5194/angeo-27-659-2009

Mitchell, D. G., Krimigis, S. M., Paranicas, C., Brandt, P. C., Carbary, J. F., Roelof, E. C., … Pryor, W. R. (2009). Recurrent energization of plasma in the midnight-to-dawn quadrant of Saturn's magnetosphere, and its relationship to auroral UV and radio emissions. *Planetary and Space Science*, *57*(14-15), 1732–1742. https://doi.org/10.1016/j.pss.2009.04.002

Morioka, A., Miyoshi, Y., Kitamura, N., Misawa, H., Tsuchiya, F., Menietti, J. D., & Honary, F. (2012). Fundamental characteristics of field-aligned auroral acceleration derived from AKR spectra. *Journal of Geophysical Research*, *117*, A02213. https://doi.org/10.1029/2011JA017137

Morioka, A., Miyoshi, Y., Tsuchiya, F., Misawa, H., Sakanoi, T., Yumoto, K., … Donovan, E. F. (2007). Dual structure of auroral acceleration regions at substorm onsets as derived from auroral kilometric radiation spectra. *Journal of Geophysical Research*, *112*, A06245. https://doi.org/10.1029/2006JA012186

Mutel, R. L., Menietti, J. D., Gurnett, D. A., Kurth, W., Schippers, P., Lynch, C., … Cecconi, B. (2010). CMI growth rates for Saturnian kilometric radiation. *Geophysical Research Letters*, *37*, L19105. https://doi.org/10.1029/2010GL044940

Parker, E. N., Marshak, R. E., & Johnson, G. (1964). Interplanetary Dynamical Processes. *Physics Toda*, *17*, 72–72. https://doi.org/10.1063/1.3051487

Provan, G., Andrews, D. J., Arridge, C. S., Coates, A. J., Cowley, S. W. H., Cox, G., … Jackman, C. M. (2012). Dual periodicities in planetary-period magnetic field oscillations in Saturn's tail. *Journal of Geophysical Research*, *117*, A01209. https://doi.org/10.1029/2011JA017104

Provan, G., Andrews, D. J., Arridge, C. S., Coates, A. J., Cowley, S. W. H., Milan, S. E., … Wright, D. M. (2009). Polarization and phase of planetary-period magnetic field oscillations on high-latitude field lines in Saturn's magnetosphere. *Journal of Geophysical Research*, *114*, A02225. https://doi.org/10.1029/2008JA013782

Provan, G., Andrews, D. J., Cecconi, B., Cowley, S. W. H., Dougherty, M. K., Lamy, L., & Zarka, P. M. (2011). Magnetospheric period magnetic field oscillations at Saturn: Equatorial phase "jitter" produced by superposition of southern and northern period oscillations. *Journal of Geophysical Research*, *116*, A04225. https://doi.org/10.1029/2010JA016213

Provan, G., Cowley, S. W., Lamy, L., Bunce, E. J., Hunt, G. J., Zarka, P., & Dougherty, M. K. (2016). Planetary period oscillations in Saturn's magnetosphere: Coalescence and reversal of northern and southern periods in late northern spring. *Journal of Geophysical Research: Space Physics*, *121*, 9829–9862. https://doi.org/10.1002/2016JA023056

Provan, G., Lamy, L., Cowley, S. W. H., & Dougherty, M. K. (2014). Planetary period oscillations in Saturn's magnetosphere: Comparison of magnetic oscillations and SKR modulations in the postequinox interval. *Journal of Geophysical Research: Space Physics*, *119*, 7380–7401. https://doi.org/10.1002/2014JA020011

Smith, A. W., Jackman, C. M., & Thomsen, M. F. (2016). Magnetic reconnection in Saturn's magnetotail: A comprehensive magnetic field survey. *Journal of Geophysical Research: Space Physics*, *121*, 2984–3005. https://doi.org/10.1002/2015JA022005

Taubenschuss, U., Rucker, H. O., Kurth, W. S., Cecconi, B., Zarka, P., Dougherty, M. K., & Steinberg, J. T. (2006). Linear prediction studies for the solar wind and Saturn kilometric radiation. *Annales Geophysicae*, *24*(11), 3139–3150. https://doi.org/10.5194/angeo-24-3139-2006

Wang, Z., Gurnett, D. A., Fischer, G., Ye, S. Y., Kurth, W. S., Mitchell, D. G., … Russell, C. T. (2010). Cassini observations of narrowband radio emissions in Saturn's magnetosphere. *Journal of Geophysical Research*, *115*, A06213. https://doi.org/10.1029/2009JA014847

Wu, C. S., & Lee, L. C. (1979). A theory of the terrestrial kilometric radiation. *The Astrophysical Journal*, *230*, 621–626. https://doi.org/10.1086/157120

Ye, S. Y., Fischer, G., Kurth, W. S., Menietti, J. D., & Gurnett, D. A. (2016). Rotational modulation of Saturn's radio emissions after equinox. *Journal of Geophysical Research: Space Physics*, *121*, 11,714–11,728. https://doi.org/10.1002/2016JA023281

Ye, S. Y., Gurnett, D. A., Fischer, G., Cecconi, B., Menietti, J. D., Kurth, W. S., … Lecacheux, A. (2009). Source locations of narrowband radio emissions detected at saturn. *Journal of Geophysical Research*, *114*, A06219. https://doi.org/10.1029/2008JA013855

Ye, S. Y., Menietti, J. D., Fischer, G., Wang, Z., Cecconi, B., Gurnett, D. A., & Kurth, W. S. (2010). Z mode waves as the source of saturn narrowband radio emissions. *Journal of Geophysical Research*, *115*, A08228. https://doi.org/10.1029/2009JA015167

Zarka, P., Cecconi, B., & Kurth, W. S. (2004). Jupiter's low-frequency radio spectrum from Cassini/Radio and Plasma Wave Science (RPWS) absolute flux density measurements. *Journal of Geophysical Research*, *109*(A9), A09S15. https://doi.org/10.1029/2003JA010260

Zarka, P., & Genova, F. (1983). Low-frequency Jovian emission and solar wind magnetic sector structure. *Nature*, *306*(5945), 767–768. https://doi.org/10.1038/306767a0

Zarka, P., Lamy, L., Cecconi, B., Prangé, R., & Rucker, H. O. (2007). Modulation of Saturn's radio clock by solar wind speed. *Nature*, *450*(7167), 265–267. https://doi.org/10.1038/nature06237

Zieger, B., & Hansen, K. C. (2008). Statistical validation of a solar wind propagation model from 1 to 10 AU. *Journal of Geophysical Research*, *113*, A08107. https://doi.org/10.1029/2008JA013046